Synthesis, Structure, and Electronic and Physical Properties of Tl_2TeS_3, the First Characterized Thallium(I) Thiotellurate(IV)

Franziska Rieger and Anja-Verena Mudring*

Anorganische Chemie, Ruhr-Universität Bochum, Universitatstrasse 150, D-44801 Bochum, Germany

Received December 5, 2005. Revised Manuscript Received October 31, 2006

The crystal structure of Tl_2TeS_3 (orthorhombic, *Pnma*, No. 62, $Z = 4$, Pearson code oP24, $a = 815.5(2)$ pm, $b = 1352.6(6)$ pm, $c = 596.48(15)$ pm, 600 unique reflections with $I_o > 2\sigma(I_o)$, $R_1 = 0.0541$, $wR_2 = 0.0997$, GOF = 0.891, $T = 298(2)$ K) in a new structure type has been determined. It can be understood as a LaI_2-like arrangement of thallium cations and thiotellurite anions TeS_3^{2-}. With a direct band gap of 1.61 eV and an indirect band gap of 0.9 eV, Tl_2TeS_3 is a new material that might be useful for thermoelectrical applications. The materials band gap is significantly lower compared to similar alkali metal systems. In addition, other than alkali metal thiotellurites, Tl_2TeS_3 is not sensitive toward the atmosphere (especially moisture). A synthetic strategy for improved thermoelectrical materials in the future might be a further reduction of the band gap by introduction of transition metals in such Tl/Te/S systems. Furthermore, density functional studies indicate that effects leading to structural distortions due to the thallium $6s^2$ lone pair are less important in sulfur compounds than in the analogous oxygen compounds.

Introduction

Thiotellurates(IV) are still a mainly unexplored class of compounds, although they might exhibit a number of interesting physical properties. So far only a few thiotellurites have been structurally characterized: Li_2TeS_3,[1] K_2TeS_3,[2] $K_3(SH)TeS_3$,[3] Ag_2TeS_3,[4] $BaTeS_3$,[5] $(NH_4)_2TeS_3$,[6] and $[PPh_4]_2[TeS_3]$.[7] With transition metals, compounds such as $Cs_6Cu_2(TeS_3)_2(S_6)_2$,[8] $AMTeS_3$ (M = K, Rb, Cs; M = Cu, Ag),[9] $A_2Mn(TeS_3)_2$ (A = Rb, Cs),[10] $CuClCu_2TeS_3$,[11] $(CuI)_3Cu_2TeS_3$, and $(CuI)_2Cu_2TeS$[12] were reported. In contrast, the class of oxotellurites is comparatively well-explored and compounds of the composition M_2TeO_3 with M = Li, Na, K, Rb, Cs, Tl, and Ag or $MTeO_3$ with M = Mg, Sr, Ba, Pb, Mn, Co, Ni, Cu, Zn, Cd, Hg, and UO^{2+} containing the ψ-tetrahedral anion TeO_3^{2-} are well-known.[13] So far for thiotellurites, the isolated ψ-tetrahedral TeS_3^{2-} unit is the only known species. For oxotellurites, however, higher condensated anionic units as $Te_2O_5^{2-}$ (dimers) in, for example, $MnTe_2O_5$[14] or $Te_3O_8^{4-}$ (trimers, C.N. of 3 and 4 around tellurium) in, for example, $Zn_2Te_3O_8$[15] and $Te_4O_9^{4-}$ (tetramers) in $Cs_2Te_4O_9$[16] have been described. Furthermore, the orthotellurite(IV) anion TeO_4^{4-}, a ψ-square pyramid, has been observed in $Co_6Te_5O_{16}$.[17]

In our ongoing efforts to explore the structural diversity in ternary thallium/chalcogenide systems, we are now able to synthesize and structurally characterize the first thallium thiotellurite(IV). Motivation for this research came not only from structural chemistry. It is well-known that the chemistry of alkali metals and thallium bear close resemblance. Some alkali metal chalcogenides show good thermoelectric properties. The (dimensionless) figure of merit for thermoelectric materials is given by $ZT = (S^2/\rho\kappa)T$, where S is the thermopower, ρ the electrical resistivity, κ the thermal

* Corresponding author. Fax: (49) 234 32 14951. E-mail: anja.mudring@rub.de. Web: http://www.anjamudring.de.

(1) Preitschaft, Ch.; Zabel, M.; Pfitzner, A. *Z. Anorg. Allg. Chem.* **2005**, *631*, 1227.
(2) Rumpf, C.; Naether, C.; Bensch, W. *Acta Crystallogr., Sect. C* **1999**, *55*, 1046.
(3) Dittmar, G.; Schäfer, H. *Z. Anorg. Allg. Chem.* **1978**, *439*, 212.
(4) Pertlik, F. *Monatsh. Chem.* **1997**, *128*, 157.
(5) Jumas, P. J.; Ribes, M.; Maurin, M.; Philippot, E. *Acta Crystallogr., Sect. B* **1976**, *32*, 444.
(6) Gerl, H.; Eisenmann, B.; Roth, P.; Schäfer, H. *Z. Anorg. Allg. Chem.* **1974**, *407*, 135.
(7) Rubenheim, W.; Frenzen, G.; Müller, U. *Z. Anorg. Allg. Chem.* **1994**, *620*, 1046.
(8) McCarthy, T. J.; Zhang, X.; Kanatzidis, M. G. *Inorg. Chem.* **1993**, *32*, 2944.
(9) Zhang, X.; Kanatzdis, M. G. *J. Am. Chem. Soc.* **1994**, *116*, 1890.
(10) Zhang, X.; Kanatzdis, M. G. *Inorg. Chem.* **1994**, *33*, 1238.
(11) Pfitzner, A. *Inorg. Chem.* **1998**, *37*, 5164. Pfitzner, A.; Reiser, S.; Nilges, T.; Kockelmann, W. *J. Solid State Chem.* **1999**, *147*, 170.
(12) Pfitzner, A.; Zimmerer, S. *Angew. Chem.* **1997**, *109*, 1031.
(13) Kohn, K.; Inoue, K.; Horie, O.; Akimoto, S. *J. Solid State Chem.* **1976**, *18*, 27. Loopstra, B. O.; Brandenburg, N. P. *Acta Crystallogr.* **1978**, *34*, 1335. Folger, F. *Z. Anorg. Allg. Chem.* **1975**, *411*, 103. Folger, F. *Z. Anorg. Allg. Chem.* **1975**, *411*, 111. Kocak, M.; Platte, C.; Troemel, M. *Z. Anorg. Allg. Chem.* **1979**, *453*, 93. Lindqvist, O. *Acta Chem. Scand.* **1972**, *26*, 1423. Hanke, K. *Naturwissenschaften* **1967**, *54*, 199. Mariolacos, K. *Anz. Öster. Akad. Wiss. Math.−Naturwiss. Klasse* **1969**, *106*, 129. Philippot, E.; Maurin, M. *Rev. Chim. Min.* **1976**, *13*, 162. H. J. Thuemmel, R. Hoppe, *Z. Naturforsch. B* **1974**, *29*, 28. Kuban, R. J. *Cryst. Res. Technol.* **1983**, *18*, 85. Loopstra, B. O.; Goubitz, B. O. K. *Acta Crystallogr., Sect. C* **1986**, *42*, 520. Kraemer, V.; Brandt, G. *Acta Crystallogr., Sect. C* **1985**, *41*, 1152. Sciau, P.; Lapasset, J.; Moret, J. *Acta Crystallogr.* **1986**, *42*, 1688. Kraemer, V.; Brandt, G. *Acta Crystallogr.* **1986**, *42*, 917. Andersen, L.; Langer, V.; Stroemberg, A.; Stroemberg, D. *Acta Crystallogr.* **1989**, *45*, 344. Elerman, Y. *Phase Transitions* **1992**, *8*, 127. Masse, R.; Guitel, J. C.; Trodjman, I. *Mater. Res. Bull.* **1980**, *15*, 431. Frit, B.; Mercurio, D. *Rev. Chim. Min.* **1980**, *17*, 192. Pertlik, F. *J. Solid State Chem.* **1987**, *71*, 291. Grice, J. D. *Canad. Min.* **1989**, *27*, 133. Frit, B.; Mercurio, D.; Thomas, P.; Champarnaud-Mesjard, J. C. Z.; *Kristallogr.−New Cryst. Struct.* **1999**, *214*, 439. Rieger, F. Mudring, A.-V. Manuscript in preparation.
(14) Walitzi, E. M. *Naturwissenschaften* **1964**, *51*, 334.
(15) Hanke, K. *Naturwissenschaften* **1966**, *53*, 273.
(16) Loopstra, B. O.; Goubitz, K. *Acta Crystallogr., Sect. C* **1986**, *42*, 520.
(17) Troemel, M.; Scheller, T. *Naturwissenschaften* **1973**, *60*, 103.

10.1021/cm0526866 CCC: $37.00
Published on Web 12/15/2006

conductivity, and T the absolute temperature.[18] In contrast to the (non-radioactive) alkali metals, thallium is less electropositive and heavier, which might lead to materials that have a higher electrical conductivity ρ and at the same time a lower thermal conductivity κ, hence, improved thermoelectric properties. These considerations have recently led to an increased interest in the field of thallium chalcogenides.[19] Indeed, for example, Tl_2SnTe_5 has a figure of merit at room temperature in the range of Bi_2Te_3, the material that to date is used in thermoelectric cooling devices.[20] Other promising compounds in this field include Tl_9BiTe_6[21] and $TlSbTe_2$.[22]

However, an effect that might crucially influence the physical properties of thallium chalcogenides is the $6s^2$ lone pair, which may become stereochemically active or not. We were recently able to show that structural distortions in thallium coordination compounds that are traditionally attributed to a stereochemical active lone pair originate not from an s−p hybridization on the thallium(I) cation to give the lone pair a structural directionality but from the tendency to minimize unfavorable anti-bonding interactions of the $6s^2$ electron pair of thallium with its bonding partner.[23] Thus, our investigation of Tl_2TeS_3 deals not only with synthesis, structure, and physical properties, such as the band gap, but also with the electronic properties of the new material with respect to the heavy metal lone pair.

Experimental Section

Materials. Thallium(I) carbonate (99.95%, Johnson Matthey Alfa Products), tellurium (99.8%, Aldrich), thallium rod (99.9%, Strem Chemicals), sulfur sublimed (99%, Strem Chemicals).

Experimental. Tl_2TeS_3 can be synthesized either by the reaction of stoichiometric amounts of the elements in a flame-sealed silica tube at 493 K or by a solvothermal reaction of thallium(I) carbonate, Tl_2Te_3, and sulfur in methanol. In the first case, phase-pure samples can be easily obtained that are used for all property measurements. The latter synthetic route leads to high-quality single crystals. Dark red to black rectangular plates with the metallic luster of Tl_2TeS_3 were obtained by reacting 50.0 mg (0.107 mmol) of Tl_2CO_3, 200.1 mg (0.253 mmol) of Tl_2Te_3, and 106.4 mg (3.31 mmol) of sulfur in 0.4 mL of methanol in a sealed glass ampule at 433 K and subsequently cooling the solution to room temperature at 1 K/h. The hydrothermally synthesized product contains mainly Tl_2TeS_3 besides unreacted sulfur, $Tl_2S_2O_3$, and β-Tl_2SO_4. The product can be separated from the sulfates by treating it with hot water.

To avoid contamination of the laboratory with thallium samples in case of a burst of the glass ampoules, all reaction containers were jacketed by steel containers with screw tops.

Crystal Structure Analysis. A few crystals were selected and sealed in thin-walled glass capillaries of 0.3 mm outer diameter and checked by Laue photographs for their quality. The best specimen was used to collect a complete intensity data set with the aid of a single-crystal X-ray diffractometer (Stoe image plate diffraction system, IPDS) at 298(2) K. For data collection and treatment and for structure solution and refinemen,t see Tables 1 and 2. Analysis of the reflection conditions reveals the possible

Table 1. Single X-ray Crystal Data Collection and Treatment

empirical formula	Tl_2TeS_3
fw (amu)	632.52
space group; Z	*Pnma*; 4
a (pm)	815.5(2)
b (pm)	1352.6(6)
c (pm)	596.48(15)
V (Å^3 mol^{-1}); ρ_{xray} (mg m^{-3})	657.9(4); 6.385
data collection	IPDS, Stoe, Darmstadt; MoKα_1 (λ = 71.073 pm); graphite monochromator; 125 images, $\Delta\varphi = 2°$
θ ranges	$2.5° \le q \le 28°$ $-7 < h < 7$ $-10 < k < 10$ $-17 < l < 17$
T (K)	298(2)
F(000)	1048
corrections	Lorentz, polarization, numerical absorption correction, X-Shape, X-Red[26]
abs coefficient (mm^{-1})	54.081
transmission T_{min}/T_{max}	0.0216/0.1032
structure solution and refinement	direct methods, SIR-92[24], full-matrix least-squares (F^2), SHELXL-97[25]
scattering factors	*Int. Tables for X-ray Crystallogr., Vol C*
no. of variable parameters	31
N(hkl)	4207
N'(hkl) unique with $I > 2\sigma(I)$	324
$R(F)_N$; $R(F)_{N'}$	0.0541; 0.1088
$R_w(F^2)_N$; $R_w(F^2)_{N'}$	0.0997; 0.1136
GOF	0.891

[a] $R_w(F^2) = \sqrt{\sum w(F_o^2 - F_c^2)^2 / \sum w(F_o^2)^2}$; $R(F) = \sum ||F_o| - |F_c|| / \sum |F_o|$.

Table 2. Atomic Coordinates ($x \times 10^{-4}$) and Equivalent Isotropic Displacement Factors U_{eq}[a] for Tl_2TeS_3

atom	Wyckoff	x/a	y/b	z/c	U_{eq} ($\times 10^{-1}$ pm^2)
Tl	8*d*	−1794(2)	5794(1)	3146(2)	45(1)
Te	4*c*	1097(3)	7500	7420(4)	35(1)
S1	4*c*	756(13)	7500	3460(20)	34(3)
S2	8*d*	−553(10)	6102(7)	8324(14)	38(2)

[a] $U_{eq} = 1/3[U_{22} + 1/\sin^2\beta(U_{11} + U_{33} + 2U_{13}\cos\beta)]$.

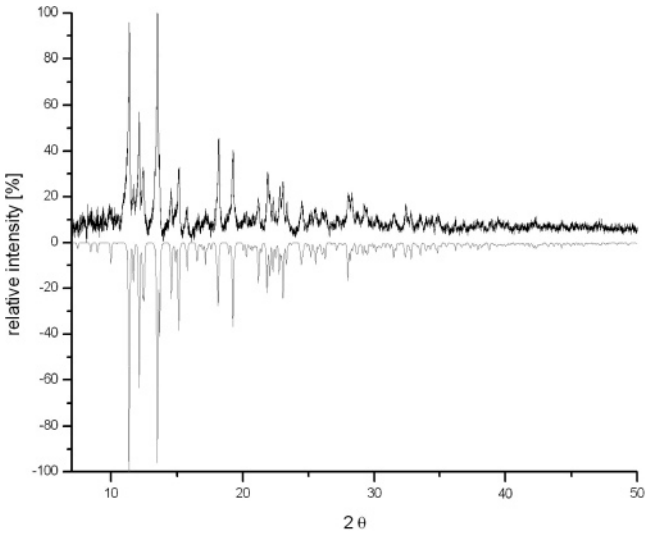

Figure 1. X-ray powder diffraction pattern of Tl_2TeS_3 prepared from the elements in a sealed silica tube.

(18) Goldsmid, H. *CRC Handbook of Thermoelectrics*; CRC Press: Boca Ration, FL, 1995.
(19) McGuire, M. A.; Reynolds, Th. K.; DiSalvo, F. J. *Chem. Mater.* **2005**, *17*, 2975. McGuire, M. A.,; Scheidemantel, Th. J.; Badding, J. V.; DiSalvo, F. J. *Chem. Mater.* **2005**, *17*, 6186.
(20) Yim, W. Y.; Rosi, F. D. *Solid-State Electron.* **1972**, *15*, 1121.
(21) Wölfing, B.; Kloc, C.; Tebuner, J.; Bucher, E. *Phys. Rev. Lett.* **2001**, *86*, 4350.
(22) Kurosake, K.; Uneda, H.; Muta, H.; Yamanaka, S. *J. Alloys Compd.* **2004**, *376*, 43.
(23) Mudring, A.; Rieger, F. *Inorg. Chem.* **2005**, *44*, 6240. Mudring, A.-V. *Eur. J. Inorg. Chem.* **2007**, in press.

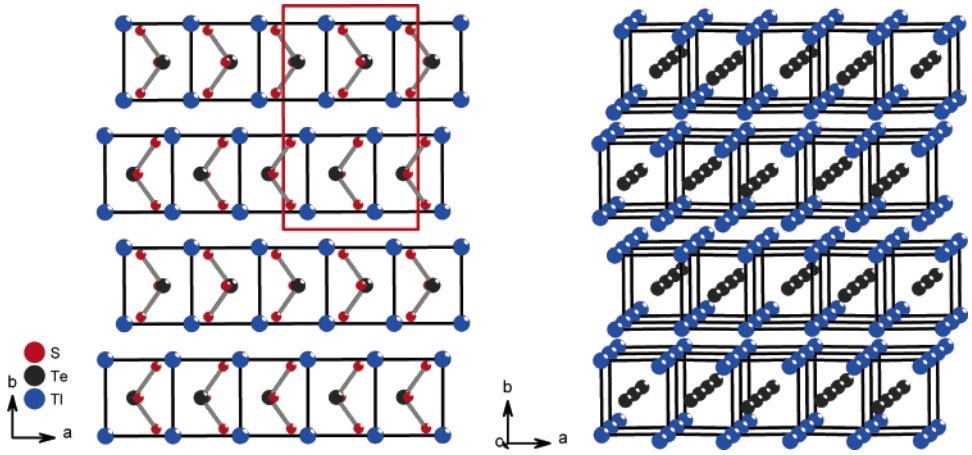

Figure 2. Analogies of the crystal structures of Tl_2TeS_3 (≡ $(TeS_3)Tl_2$) and LaI_2.

space groups $Pn2_1a$ (No. 33, noncentrosymmetric) and *Pnma* (No. 62, centric). Structure solution and refinement give no indication for a noncentrosymmetric structure. Structure solution with direct methods (SIR-92[24]) reveals the crystallographic positions of all atoms. Subsequent structure refinement was undertaken with the program SHELXL-97.[25]

Further details of the structure refinement may be obtained from the Fachinformationszentrum Karlsruhe, D-76344 Eggenstein-Leopoldshafen, crysdata@FIZ-Karlsruhe.de, referring to CSD 391285, the authors, and the journal citation. For drawings of the crystal structure, the program Diamond (Crystal Impact, Bonn, Germany, 1995) was used.

Powder X-ray Diffraction. Powder X-ray diffraction data were obtained using an image plate Guinier camera (Huber G670) diffractometer (Mo $K\alpha_1$, image plate).

Tl_2TeS_3: orthorhombic, $a = 815.9(6)$ pm, $b = 1348.3(7)$ pm, $c = 597.7(3)$ pm (Mo $K\alpha_1$, 293 K, 23 indexed lines) (see Figure 1).

IR and Raman Spectroscopy. IR spectra of the solid were recorded using a IFS-66V-S Fourier transform IR spectrometer; samples were pressed in a polyethylene matrix for measurement. Raman spectra were recorded with a FRA 106-S Fourier transform Raman spectrometer. Raman samples were measured in glass capillaries with an inner diameter of 0.1 cm and 0.15 mm wall thickness.

Raman (cm^{-1}): 338 (s), 309 (m), 189 (w), 180 (m), 154 (m), 114 (w).

FIR (cm^{-1}): 342 (w), 315 (m), 189 (m), 164 (m), 125 (m), 67 (w), 57 (m), 48 (w).

UV−Visible−Near-IR Spectra. Visible−NIR absorption spectra were measured at room temperature on a Cary 05E double-beam spectrometer (Varian, Palo Alto, USA). The sample was ground into fine powder and placed as a thin layer between two pieces of commercial (polypropylene) "sticky tape".

Conductivity Measurements. The temperature dependence of the specific electrical conductivity was measured according to the four-point-AC method.[26] A Tl_2TeS_3 powder pellet was first sintered at 200 °C for 48 h under argon and then cut to a rectangular parallel epiped with the dimensions of $0.8 \times 0.5 \times 0.1$ cm^3. Finally, the samples were contacted with copper wires with silver paste.

Thermal Measurements. Differential scanning calorimetry (DSC) was performed with a computer-controlled Netzsch Phoenix DSC F1 thermal analyzer with argon as protection gas. Thermal analysis was carried out in pierced gold pans. The DSC run included heating to 350 °C at a rate of 10 °C/min and subsequent cooling to 20 °C at 10 °C/min. The experimental data are displayed in such a way that exothermic peaks occur at negative heat flow and endothermic peaks at positive heat flow.

Computational Details. Ab initio calculations of the electronic structure of the Tl_2TeS_3 were carried out within the framework of the DFT method using the FP−LAPW (full potential−linear augmented plane wave) method[27] as embodied in the WIEN2k program package.[28] For treatment of the electron correlation within the generalized gradient approximation (GGA), we used the exchange−correlation potential with the parametrization by Perdew et al.[29] For valence states, relativistic effects are included through a scalar relativistic treatment,[30] core electrons are treated as fully relativistic;[31] 1000 independent *k*-points were calculated in the Brillouin zone.

To analyze the bonding in Tl_2TeS_3, we carried out further calculations with the Stuttgarter LMTO-ASA program package, which uses the tight-binding linear-muffin-tin orbital (LMTO) method in the local density (LDA) and atomic sphere (ASA) approximation.[32,33] All relativistic effects except spin−orbit coupling were taken into account using scalar relativistic approximations. The calculations include corrections for the neglect of the interstitial regions and the partial waves of higher order. To reduce the overlap of atomic spheres (AS), we added empty interstitial spheres to the crystal potential and the basis set. The construction of the atomic sphere radii that was performed according to an automatic procedure[34] of the program package until the empty space was sufficiently filled yielded unacceptably high values for thallium, thus its value was set by hand to 3.59. The automatic routine yielded a radius of 2.83 for Te, 2.48 for S1, and 2.48 for S2. The muffin

(24) Altomare, A.; Cascarano, G.; Giacovazzo, C.; Guagliardi, A. *SIR92: A Program for Crystal Structure Solution*; *J. Appl. Crystallogr.* **1993**, *26*, 343.
(25) Sheldrick, W. S.; *SHELXL-97*; Universität Göttingen: Göttingen, Germany, 1997.
(26) *X-RED, X-Shape*; Stoe & Cie: Darmstadt, Germany, 2002.
(27) Altomare, A.; Cascarano, G.; Giacovazzo, C.; Guagliardi, A. *SIR92: A Program for Crystal Structure Solution*; *J. Appl. Crystallogr.* **1993**, *26*, 343.
(28) Sheldrick, W. S. *SHELXL-97*; Universität Göttingen: Göttingen, Germany, 1997.
(29) Mirgel, R. Ph.D. Disseration, Universität zu Köln, Köln, Germany, 1986.
(30) Singh, D. H. *Planewaves, Pseudopotentials, and the LAPW Method*; Kluwer Academic Press: Boston, 1994. Blaha, P.; Schwarz, K.; Soratin, P.; Trickey, S. B. *Comput. Phys. Commun.* **1990**, *59*, 399.
(31) Blaha, P.; Schwarz, K.; Luitz, U. *WIEN2k*; Vienna University of Technology: Vienna, Austria, 2001.
(32) Perdew, J. P.; Burke, S.; Ernzerhof, M. *Phys. Rev. Lett.* **1996**, *77*, 3865.
(33) MacDonald, A. H.; Pickett, W. E.; Koelling, D. D. *J. Phys. Chem. C* **1980**, *13*, 2675.
(34) Desclaux, J. P. *Comput. Phys. Commun.* **1969**, *1*, 216.

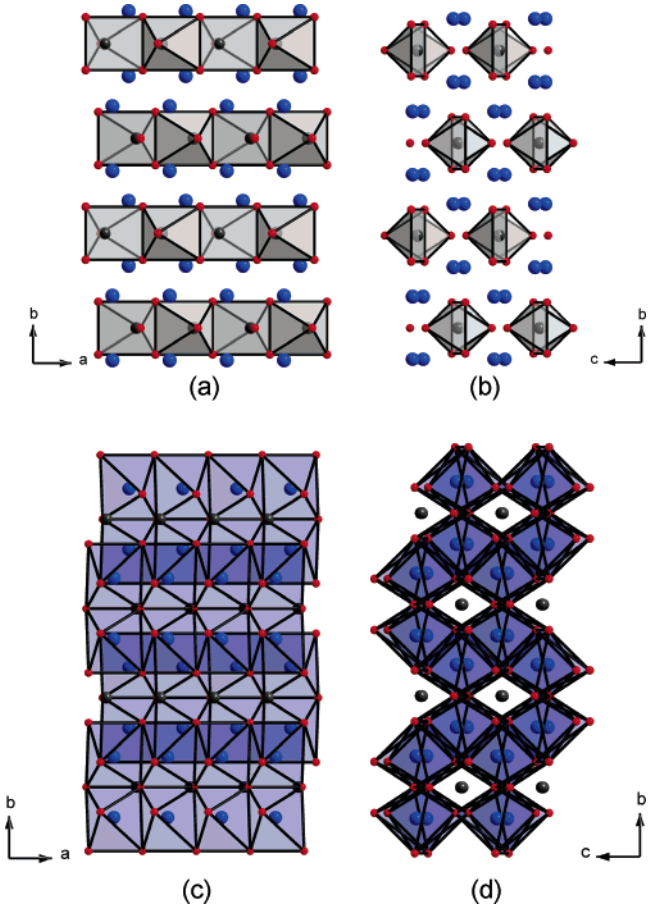

Figure 3. Structure description of Tl_2TeS_3 as (distorted) [TeS_6] octahedra (a and b) and [TlS_6] octahedra (c and d).

Table 3. Selected Interatomic Distances (pm) and Angles (deg) in Tl_2TeS_3

Te−S1	237.8(12)	×1	Tl−Te	390.0(9)	×2
Te−S2	238.3(9)	×2	Tl−Te	416.9(3)	×2
Tl−S2	307.7(8)	×1	S(1)−Te−S(2)	99.1(2)	×2
Tl−S1	311.2(7)	×1	S(2)−Te−S(2)	105.1(3)	×1
Tl−S1	320.0(8)	×1			
Tl−S2	327.7(8)	×1			
Tl−S2	331.8(9)	×1			
Tl−S2	335.7(9)	×1			

tin radii for the empty spheres ranged from 2.23 down to 1.11. The basis set of short-ranged, atom-centered TB-LMTOs contained *n*s, *n*p, and *n*d wavefunctions for Tl ($n = 6$), Te ($n = 5$), and S ($n = 3$). The *n*d waves were included only in the tails of the LMTOs according to the Löwdin downfolding procedure.[35] For the larger empty spheres ($r > 2$) 1s-, 2s-, and 2p-like functions were taken into account; the latter two were downfolded, and 250 *k*-points were calculated in the Brillouin zone.

All reciprocal space integrations are carried out using the tetrahedron method.[36] To examine in detail the effect of the anion on the electronic density of states, we have calculated the partial ion *l* and *m* quantum number decomposed electronic density of states. They were calculated by projecting the wave functions onto spherical harmonics centered on each atom (PDOS = projected

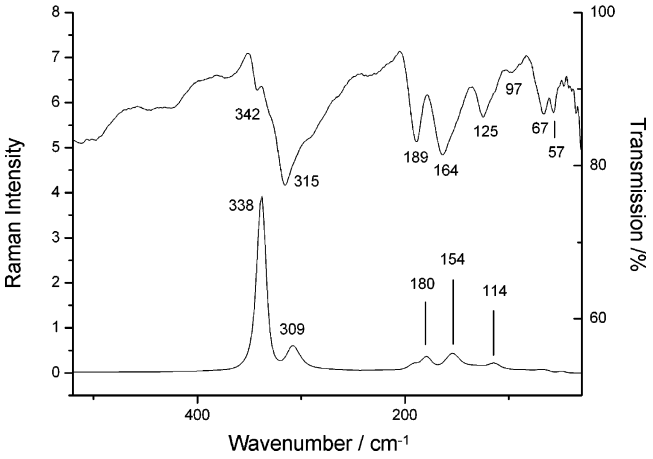

Figure 4. FIR spectrum (top) and Raman spectrum (bottom) of Tl_2TeS_3.

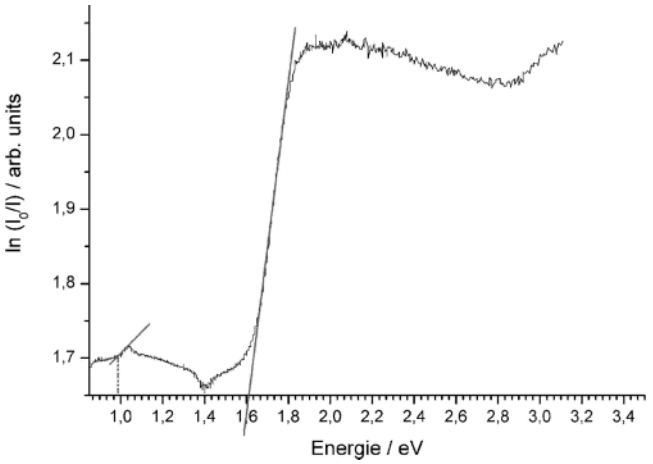

Figure 5. UV−visible spectrum of Tl_2TeS_3.

density of states). For bond analysis, the crystal orbital Hamiltonian population (COHP) method is used together with its integration, the ICOHP.[37]

In all cases, the structural data were employed as reported and the highest occupied level is always chosen as the level of reference for the energy.

Results and Discussion

Crystal Structure. Tl_2TeS_3 crystallizes with the orthorhombic space group *Pnma* with four formula units in the unit cell (Figure 2). The main structural feature are TeS_3^{2-} complex ions, which adopt a ψ-tetrahedral structure. The tellurium−sulfur distances of d(Te−S1) = 237.8(12) pm and d(Te−S2) = 238.3(9) pm (cf. Table 3) are slightly larger when compared to the values found in K_2TeS_3[38] (d(Te−S) = 235.0(4) pm), Ag_2TeS_3[39] (d(Te−S) = 237.3(9) pm) and $BaTeS_3$[40] (d(Te−S) = 235.8(7) pm). This may be indicative of a lower charge separation and, hence, lower ionicity in the thallium compound. Within the ψ-tetrahedral TeS_3^{2-} anion, interatomic angles of <(S(1)−Te−S(2)) = 99.1(2)° (×2) and <(S(2)−Te−S(2)) = 105.1(3)° (×1) are observed.

(35) Shriver, H. L. *The LMTO Method*; Springer-Verlag: Berlin, 1984. Jepsen, O.; Snob, M.; Andersen, O. K. *Linearized Band-Structure Methods in Electronic Band-Structure and its Applications*; Springer Lecture Note Series; Springer-Verlag: Berlin, 1987. Anderson, O. K.; Jepsen, O. *Phys. Rev. Lett.* **1984**, *53*, 2571.
(36) Tank, R. W.; Jepsen, O.; Burckhardt. A.; Andersen, O. K. *TB-LMTO-ASA Program*, version 4.7; Max-Planck-Institut für Festkörperforschung: Stuttgart, Germany, 1998.
(37) Jepsen, O.; Anderson, O. K. *Z. Phys.* **1995**, *B97*, 35.
(38) Lambrecht, W. R. L.; Andersen, O. K. *Phys. Rev. B* **1986**, *B34*, 2439. Jensen, O.; Andersen, O. K. *Z. Phys. B.* **1995**, *B97*, 35. Krier, G.; Jepsen, O.; Andersen, O. K. Max-Planck-Institute fur Festkörperforschung: Stuttgart, Germany, unpublished.
(39) Andersen, O. K.; Jespen, O. *Solid State Commun.* **1971**, *9*, 1763. Blöchl, P.; Jepsen, O.; Andersen, O. K. *Phys. Rev. B* **1994**, *34*, 16223.
(40) Dronskowski, R.; Blöchl, P. E. *J. Phys. Chem.* **1993**, *97*, 8617.

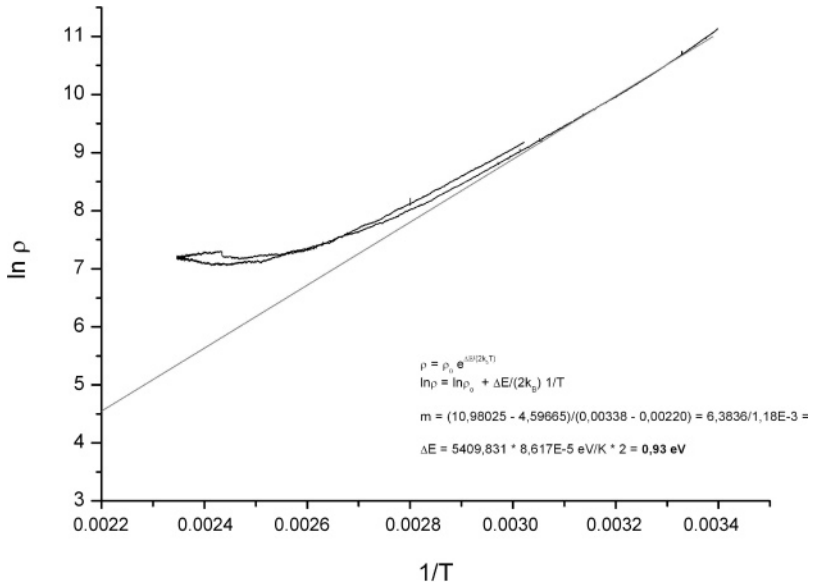

Figure 6. Temperature dependence of the electrical resistance of a Tl_2TeS_3 sample.

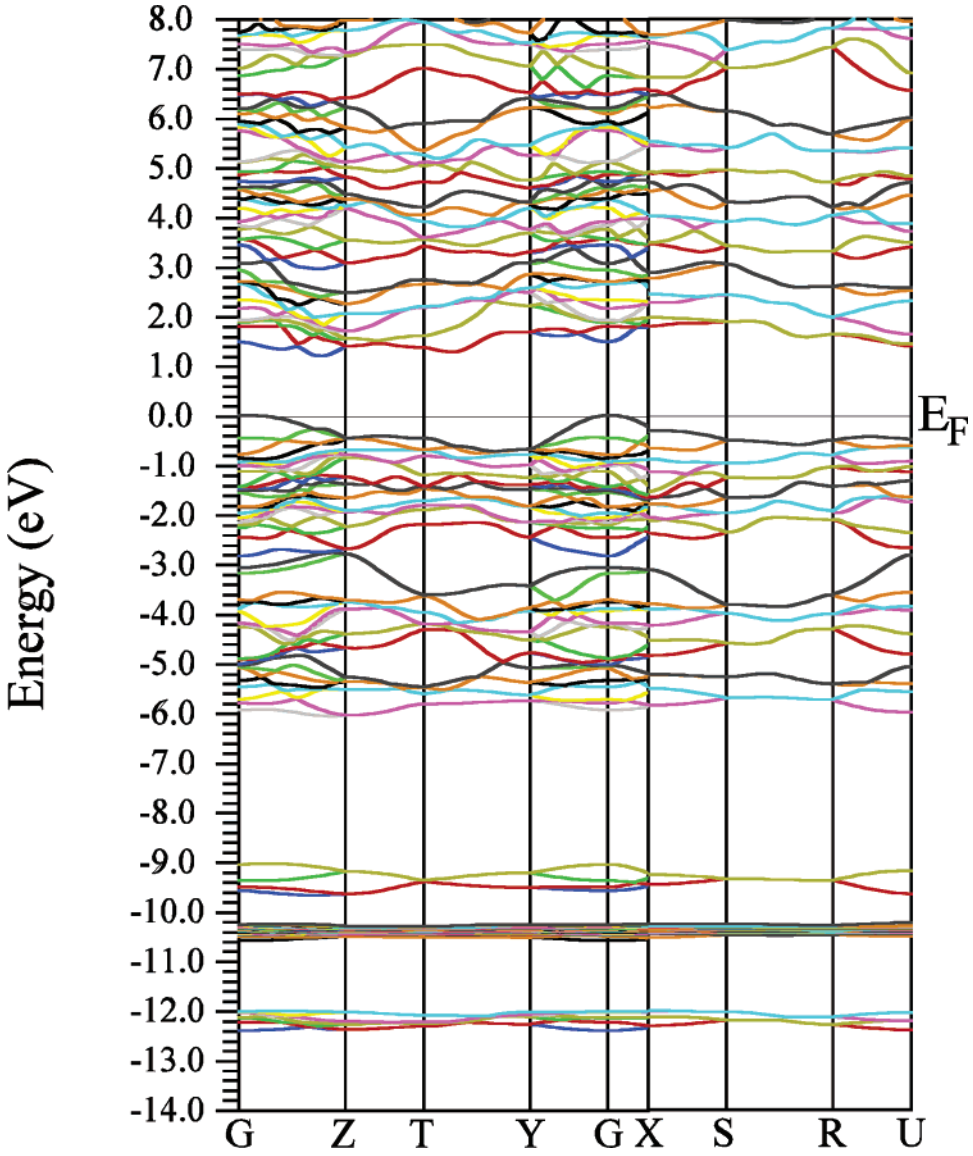

Figure 7. Band structure of Tl_2TeS_3 as obtained from full-potential WIEN2k calculations.

When compared to the bonding angles observed in other known thiotellurates(IV), the anion in Tl_2TeS_3 appears to be less symmetric (K_2TeS_3 (<(S−Te−S) = 103.10(3), 102.13(3), and 102.16(3)°), Ag_2TeS_3 (<(S−Te−S) = 97.8-

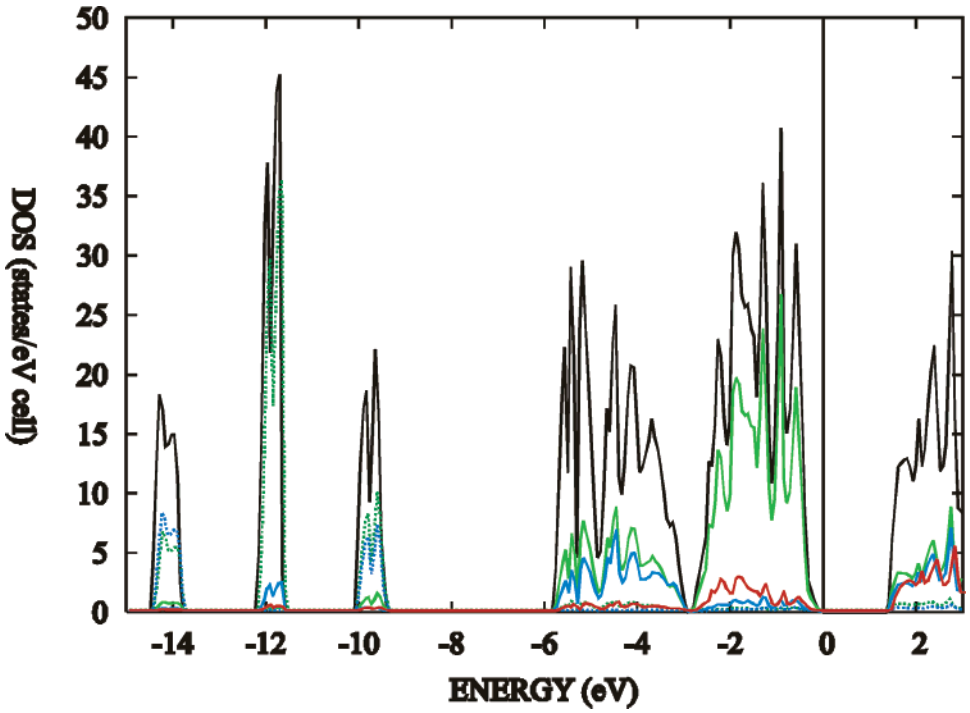

Figure 8. Total and partial density of states for Tl_2TeS_3. Dotted lines, s states;, solid lines, p states; red, Tl; blue, Te; green, S (FP-LAPW).

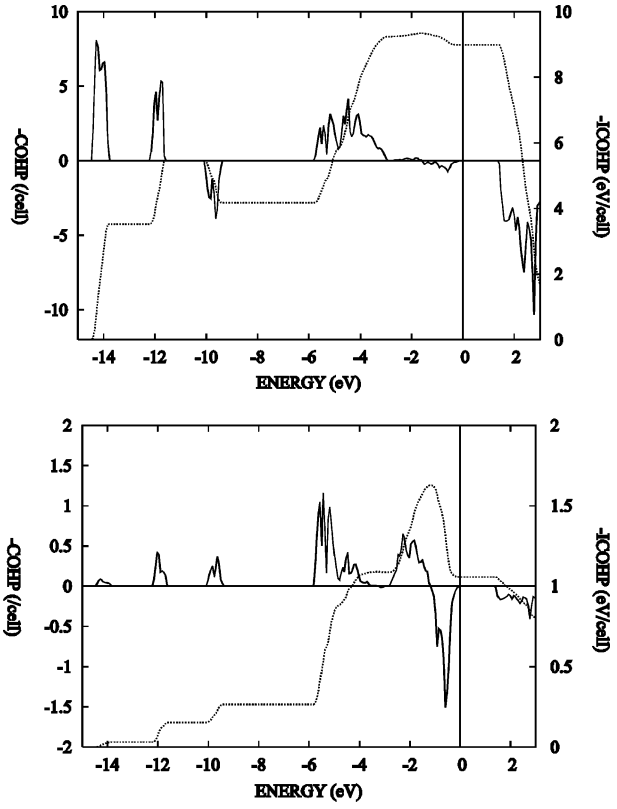

Figure 9. COHP (solid line) and ICOHP (dotted line) for the Te−S (left) and Tl−S bond (right) in Tl_2TeS_3 (LMTO-ASA).

(1), 98.28(9), and 100.38(9)°) and $BaTeS_3$ (<(S−Te−S) = 100.44(16)° (×2), 101.16(25)°).

Each TeS_3^{2-} anion is surrounded by an only slightly distorted cube of thallium cations (Figure 2, left). These cubes are connected via four faces to form sheets parallel to the crystallographic *c*-axis. The stacking sequence of the thallium 4^4 nets is AABB. Thus, the structural arrangement bears a close resemblance to the structure of $LaI_2/CuTi_2$[41] (cf. Figure 2, right), with TeS_3^{2-} occupying the lanthanum positions and Tl^+ the iodine positions in LaI_2.

Taking into account the next nearest sulfur atoms, the coordination sphere of tellurium(IV) gets completed by three additional S^{2-} anions at distances of 2 × 335.2(9) and 1 × 361(1) pm to a distorted octahedron (Figure 3). Tl^+ shows a less distorted octahedral coordination by sulfur with a mean Tl−S interatomic distance of 322.4 pm. The [TeS_6] octahedra are connected via common edges to chains that run parallel to the crystallographic *a*-axis (panels a and b of Figure 3). The [TlS_6] octahedra form edge-sharing double strands that also run parallel to the *a*-axis but are connected via common edges to two sets of double strands in the next layer (panels c and d of Figure 3) creating a three-dimensional network with open channels that are filled by tellurium(IV).

Infrared and Raman Spectroscopy. The TeS_3^{2-} anion has C_s symmetry. It is expected to observe in the vibrational spectra a symmetric and a asymmetric Te−S1 streching vibration together with a Te−S2 stretching vibration within the mirror plane. Because of the similar bond length, the force constants of the Te−S1 and Te−S2 bonds are expected to be similar. As a consequence, the vibrations of the complex anion can approximately be described as the $2A_1$ + 2E modes of a molecule with C_{3v} symmetry. Thus, the TeS_3^{2-} anion is expected to give rise to a symmetric and an asymmetric Te−S stretching vibration. The Raman spectrum (Figure 4, bottom line) shows well-resolved bands at 338 cm^{-1} for the ν_s (Te−S) and 309 cm^{-1} for the ν_{as} (Te−S) stretching vibration. As expected, the intensity ratios for the respective modes are reversed when comparing the Raman with the IR spectrum (Figure 4, top line). The bands between 200 and 100 cm^{-1} can be attributed to S−Te−S bending

(41) Rumpf, A. Naether, C.; Bensch, W. *Acta Crystallogr., Sect. C* **1999**, *55*, 1046.

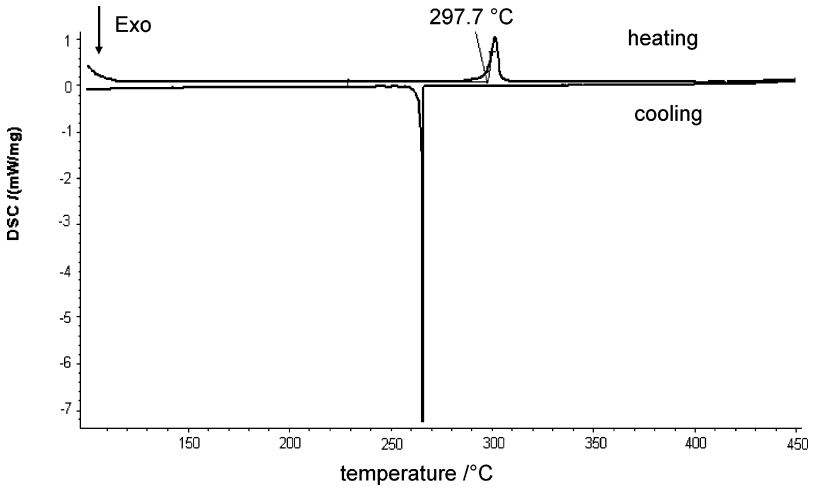

Figure 10. Thermogram of Tl_2TeS_3.

deformations. As the Tl−S interactions are much weaker, motions of the Tl−S substructures occur at even lower frequencies (<100 cm^{-1}).

UV−visible−Near-Infrared Spectroscopy. The optical properties of Tl_2TeS_3 were determined by studying the absorption spectrum in the UV−visible−NIR region. The compound exhibits a sharp direct optical gap ($k = 0$) with a high-intensity absorption in the visible region of the spectrum (Figure 5). The band gap was estimated from extrapolation of the absorption edge on the energy axis of an A^2 vs E plot (A = absorption in arbitrary units, E = energy in eV) to a value of 1.61 eV. Although still a wide-gap semiconductor, the optical band gap of Tl_2TeS_3 is lower than in most quaternary alkali metal thiotellurites such as $A_2Mn(TeS_3)_2$ (A = Rb, Cs)[42] or $AMTeS_3$ (A = K, Rb, Cs; M = Cu, Ag),[43] which show optical band gaps from 1.95 to 2.4 eV. In addition, a second absorption with a substantionally lower intensity could be detected at 0.9 eV that can be attributed to a indirect band gap ($k \neq 0$).

Conductivity Measurements. Evaluation of the temperature dependence of the resistance of a Tl_2TeS_3 sample in the temperature range between 294 and 410 K shows an indirect, elctrical band gap of 0.93 eV, which is in good agreement with the optical data (Figure 6).

Theory. Calculations carried out within the framework of density functional theory predict a direct band gap of 1.5 eV and an indirect band gap of 1.1 eV, which matches astonishingly well the optically determined gap when taking into account that one of the major failures of density functional theory is the underestimation of band gaps (Figure 7). The observed optical band gap corresponds, according to the calculations, to transitions that start from bands belonging mostly to sulfur lone pairs (p-states) into empty Tl and Te bands of p-character (Figure 8). The tellurium-centered bands originate from the Te−S anti-bonding interactions (Figure 9).

The theoretical calculations undertaken can also explain why thallium adopts in Tl_2TeS_3, in contrast to Tl_2TeO_3,[44] a comparatively highly symmetric surrounding. Whereas in Tl_2TeS_3, the coordination polyhedron formed by sulfur around thallium resembles a weakly distorted octahedron, in the analogous oxo-tellurite ψ-square, bipyramidal [TlO_4] units are found. The considerably lower degree of distortion in the sulfur compound is due to the energetical mismatch of the 6s Tl and 3p S atoms. The 6s Tl orbitals are shifted downward in energy by relativistic effects, and therefore, their separation on the energy scale from the 3p S atoms is fairly large, leading only to a comparatively weak covalent interaction. Thus, the minimization of anti-bonding 6s Tl/3p S lone pair interactions by structural distortions is less favored. Instead, a higher symmetric structure with a larger Madelung factor, hence, Coulombic interactions, is obviously preferred.

Thermal Analysis. The thermal behavior of Tl_2TeS_3 was investigated by differential scanning calorimetry (DSC). Figure 10 shows the thermogram of the compound. At 299 °C (onset), an endothermic peak due to the melting of the compound is observed. Up to 450 °C, the compound shows no signs of thermal decomposition. Over a temperature range of −70 °C to the melting point, no solid−solid phase transitions could be detected.

Conclusions

The direct optical band gap of Tl_2TeS_3 is significantly lower than in most quaternary systems such as $A_2Mn(TeS_3)_2$ (A = Rb, Cs)[45] or $AMTeS_3$ (A = K, Rb, Cs; M = Cu, Ag).[46] These show optical band gaps from 1.95 to 2.4 eV. This feature is due to the less electropositive character of thallium when compared to the alkali metals. In addition, a indirect electrical band gap of 0.9 eV was observed that might render Tl_2TeS_3 a thermoelectric material. A synthetic strategy for obtaining a better material might be to look for quaternary transition metal thiotellurites with thallium instead of alkali metals. Another large advantage of thallium compounds over alkali metal thiotellurites is that they are not sensitive toward moisture.[47] Still, similar structures would be expected, as our theoretical calculations show that the effects leading to

(42) Pertlik, F. *Monatsh. Chem.* **1997**, *128*, 157.
(43) Jumas, P. J.; Ribes, M.; Maurin, M.; Philippot, E. *Acta Crystallogr., Sect. B* **1976**, *32*, 444.
(44) Burrow, J. H.; Maule, C. H.; Strange, P.; Tothill, J. N.; Wilson, J. A. *J. Phys. C* **1987**, *20*, 4115.
(45) Zhang, X.; Kanatzidis, M. G. *Inorg. Chem.* **1994**, *33*, 1238.
(46) Zhang, X.; Kanatzdis, M. G. *J. Am. Chem. Soc.* **1994**, *116*, 1890.

structural distortions due to the thallium $6s^2$ lone pair are less important in sulfur compounds than in the analogous oxygen compounds.

Acknowledgment. A.-V. M. thanks the BMBF and Fonds der Chemischen Industrie for support and the Deutsche Forschungsgemeinschaft for generous financial support. Dipl.-Phys. Eva Rose, Universität zu Köln, is acknowledged for carrying out the electrical conductivity measurements.

Supporting Information Available: Crystallographic information in CIF format. This material is available free of charge via the Internet at http://pubs.acs.org.

CM0526866

(47) Frit, B.; Mercurio, D. *Rev. Chim. Min.* **1980**, *17*, 192. Frit, B. Mercurio, D.; Thomas, P.; Champarnaud-Mesjard, J. C. *Z. Kristallogr.−New Cryst. Struct.* **1999**, *214*, 439. Rieger, F.; Mudring, A. V. *Inorg. Chem.* **2006**, accepted.
(48) Zhang, X.; Kanatzidis, M. G. *Inorg. Chem.* **1994**, *33*, 1238.
(49) Zhang, X.; Kanatzidis, M. G. *J. Am. Chem. Soc*. **1994**, *116*, 1890.
(50) Rumpf, A.; Naether, C.; Bensch, W. *Acta Crystallogr., Sect. C* **1999**, *55*, 1046. Preitschaft, Ch.; Zabel, M.; Pfitzner, A. *Z. Anorg. Allg. Chem.* **2005**, *631*, 1227.